Structural Chemistry and Magnetic Properties of $Nd_2BaLiRuO_7$

Jennifer A. Rodgers,[†] Peter D. Battle,*[,†] Clare P. Grey,[‡] and Jeremy Sloan[†]

Inorganic Chemistry Laboratory, Oxford University, South Parks Road, Oxford, OX1 3QR, United Kingdom, and Department of Chemistry, State University of New York at Stony Brook, Stony Brook, New York 11794-3400

Received May 2, 2005

The synthesis and characterization of a polycrystalline sample of the $n = 2$ Ruddlesden−Popper phase $Nd_2BaLiRuO_7$ are reported. X-ray and neutron diffraction show that the 6-coordinate sites are occupied by a 1:1 ordered arrangement of Li and Ru, that the 12-coordinate sites within the perovskite-like blocks are occupied by Ba, and that the cation sites on the block edges are occupied by Nd. Transmission electron microscopy shows that this compound is less susceptible to stacking faults then many other $n = 2$ phases, and ^{7}Li MAS NMR spectroscopy shows that the environment of the single Li site in the structure is well-defined. The compound is an antiferromagnet below 32 K, with ordered magnetic moments of 2.2(2) μ_B and 2.53(8) μ_B on the Ru and Nd cations respectively at 2 K.

Introduction

We have previously[1,2] discussed the relative importance of nearest-neighbor (NN) and next-nearest-neighbor (NNN) cation interactions in determining the magnetic properties of transition-metal oxides which adopt Ruddlesden−Popper (RP) structures. We subsequently prepared compounds in which 50% of the six-coordinate, B-site cations are nonmagnetic in an attempt to eliminate the NN interaction and hence to facilitate the characterization of the NNN interaction in isolation. This strategy, which was originally focused on Mn-based oxides, relied on the magnetic transition-metal cations and the diamagnetic cations in our target phases occupying the octahedral sites in a 1:1 ordered manner, a requirement that was not always satisfied. In the case of the $n = 1$ phases La_4LiMnO_8 and $La_3SrLiMnO_8$ we observed[3] 1:1 ordering of Mn and Li cations in each individual sheet of octahedra, but the stacking of these layers was random along the [001] axis of the tetragonal unit cell and hence no long-range cation ordering was observed. A similar lack of three-dimensional order was found[4] in $n = 2$ La_3LiMnO_7. Having failed to induce ordering between Li^+ and $Mn^{3+/4+}$ cations, and being aware[5] that the $n = \infty$ RP phase La_2LiRuO_6 is cation-ordered, we attempted to use the cation pair Li^+/ Ru^{5+} to induce order in $n = 1$ phases. This resulted[6] in the preparation of $La_2Sr_2LiRuO_8$ which crystallizes in a supercell of the $n = 1$ RP structure that can accommodate cation ordering on both the 6-coordinate sites and on the 9-coordinate (La^{3+}/Sr^{2+}) sites. This compounds orders magnetically at 85 K, a relatively high Néel temperature for a layered oxide in which the magnetic ion comes from the second transition series.

In this paper we report an extension of our study of Li^+/ Ru^{5+} compounds to include $n = 2$ RP phases. The only example of an $n = 2$ RP phase reported to date which exhibits a degree of ordering between cations of two different elements over the 6-coordinate B sites is La_3LiMnO_7.[7] X-ray diffraction did not reveal any B-site ordering in this composition and the structure could be refined in the space group ($I4/mmm$) associated with the majority of $n = 2$ RP phases. However, additional Bragg peaks were seen in the neutron diffraction pattern. These could be indexed in the space group $P4_2/mnm$ which allows for the rotation of the vertex-sharing octahedra but does not allow for cation ordering over the B sites. Additional diffuse scattering was apparent parallel to c^* in the electron diffraction patterns and the distribution of intensity maxima along the scattering line 01ξ was inconsistent with the space group $P4_2/mnm$ and suggestive of partial cation ordering within the crystallites. These maxima in the diffuse scattering were not seen in the related $n = 1$ phases (La_4LiMnO_8 and $La_3SrLiMnO_8$),[3] thus leading to the hypothesis that the average size of the coherently ordered structural regions is greater in the case of the $n = 2$ phase. Complete cation ordering within the perovskite bilayers was observed in high-resolution lattice images, although some disorder was observed between the layers. The 1:1 cation ordering within the bilayers was also confirmed by the detection of a single lithium environment using ^{6}Li MAS NMR. Despite the fact that the magnetic susceptibility of La_3LiMnO_7 indicated a Néel temperature of 14 K, no magnetic Bragg reflections were observed in

* To whom correspondence should be addressed. E-mail: peter.battle@chem.ox.ac.uk.
[†] Oxford University.
[‡] State University of New York at Stony Brook.

(1) Cussen, E. J.; Vente, J. F.; Battle, P. D.; Gibb, T. C. *J. Mater. Chem.* **1997**, *7*, 459.
(2) Gibb, T. C.; Herod, A. J.; Lees, S. T.; Battle, P. D. *J. Mater. Chem.* **1995**, *5*, 285.
(3) Burley, J. C.; Battle, P. D.; Gallon, D. J.; Sloan, J.; Grey, C. P.; Rosseinsky, M. J. *J. Am. Chem. Soc.* **2002**, *124*, 620.
(4) Battle, P. D.; Burley, J. C.; Gallon, D. J.; Grey, C. P.; Sloan, J. *J. Solid State Chem.* **2004**, *177*, 119.
(5) Battle, P. D.; Grey, C. P.; Hervieu, M.; Martin, C.; Moore, C. A.; Paik, Y. *J. Solid State Chem.* **2003**, *175*, 20.
(6) Rodgers, J. A.; Battle, P. D.; Dupre, N.; Grey, C. P.; Sloan, J. *Chem. Mater.* **2004**, *16*, 4257.
(7) Battle, P. D.; Burley, J. C.; Gallon, D. J.; Grey, C. P.; Sloan, J. *J. Solid State Chem.* **2003**, *177*, 119.

10.1021/cm050923z CCC: $30.25
Published on Web 07/23/2005

the low-temperature neutron diffraction pattern due to the lack of long-range ordering between the ordered bilayers. Although no known compounds contain cations of two different elements that exhibit complete ordering over the B sites, it is interesting to note that charge ordering between Mn^{3+}/Mn^{4+} in $La_2SrMn_2O_7$ in the temperature range $100 < T/K < 210$ results[8] in the formation of a superstructure that can be described in space group *Bbmm*.

In addition to studies of B-site ordering, much research to date into RP phases has focused on inducing cation ordering over the A sites of the $n = 2$ structure. A-site ordering has been observed between lanthanides and, in most cases, either strontium or calcium. Within the family $LnSr_2Mn_2O_7$, the larger Sr cation was found to exhibit a preference for the site within the perovskite blocks when Ln was a relatively small lanthanide, for example, Ho or Y.[9] The same type of ordering has been observed in $LaCa_2Mn_2O_7$ with the La ions showing a preference for the 12-coordinate site within the perovskite blocks and the smaller Ca ions showing a preference for the 9-coordinate sites on the boundaries of the blocks.[10]

We describe below the synthesis and characterization of the $n = 2$ RP phase $Nd_2BaLiRuO_7$. The contrast between the size and charge of Li^+ and Ru^{5+}, in addition to their chemical differences, might be expected to lead to some degree of chemical ordering in 1:1 mixed Li^+:Ru^{5+} $n = 2$ compounds, as is the case for $n = 1$ and $n = \infty$. Given the chessboard ordering in the *xy* plane previously observed in the B-site ordered K_2NiF_4-type compounds,[3,11−17] the most appropriate ordering scheme might be expected to be an extension of this alternate ordering throughout the two connected perovskite sheets. In the simplest case, this would require a $\sqrt{2} \times \sqrt{2} \times 1$ expansion of the basic tetragonal unit cell, and a lowering of the crystal symmetry. In addition, the presence of two types of cation, differing in both size and charge, on the A sites creates the possibility of further ordering within the crystal. As discussed above, strontium exhibits a degree of ordering on the A site with smaller lanthanides,[9,18] and the larger Ba cation was introduced into these new compounds with the aim of increasing the extent of this ordering. Barium-containing $n = 2$ RP phases are relatively rare, examples being $Ln_2BaIn_2O_7$ (Ln = La, Nd)[19] and $Gd_2BaMn_2O_7$[20] where complete A-site ordering was observed with the lanthanide situated in the rock-salt layer and the barium cation within the perovskite block. Both these compounds are tetragonal and adopt space group $P4_2/mnm$, which permits tilting of the BO_6 octahedra.

Magnetically, the ordered K_2NiF_4-type compound $La_2Sr_2LiRuO_8$ was found to exhibit strong, antiferromagnetic π superexchange within the *xy* plane. As a consequence of the increase in the dimensionality of the structure, the magnetic π superexchange in $n = 2$ RP Li/Ru phases would be expected to involve the Ru d_{xz} and d_{yz} orbitals in addition to the d_{xy} orbital, thus leading to the possibility of stronger magnetic coupling. Furthermore, the additional presence of a magnetic cation on the A sites leads to the possibility of long-range magnetic order involving both A and B sites. $Nd_2BaLiRuO_7$ thus offers a number of possibilities involving both cation ordering and magnetic ordering over two chemically distinct sites. We present below an account of the synthesis of this composition, together with a description of the structural chemistry and magnetic properties.

Experimental Section

A polycrystalline sample (∼5 g) of $Nd_2BaLiRuO_7$ was synthesized by standard high-temperature, solid-state techniques. Appropriate amounts of $BaCO_3$, Nd_2O_3, RuO_2, and Li_2CO_3 were thoroughly ground using an agate pestle and mortar. Due to the low melting point of Li_2CO_3 (723 °C) and its high volatility, an initial excess of 50% was used in each synthesis. The reactants were fired at 800 °C for 4 h, and then an additional 50% excess of Li_2CO_3 was added and intimately ground with the sample before further firing at 900 °C for 16 h.

The progress of the reaction was monitored by X-ray powder diffraction. Data suitable for Rietveld analysis were collected on the final product in Bragg−Brentano geometry on a Siemens D5000 diffractometer with monochromated Cu $K\alpha_1$ radiation, $\lambda = 1.54059$ Å, over the angular range $10 \leq 2\theta/° \leq 120$, using a step size of $\Delta 2\theta = 0.02°$. The crystallinity of the product was assessed by examining the full-width at half-maximum (fwhm) of a single reflection at $2\theta \sim 42°$. A fwhm of 0.10° or less was taken to be evidence that a highly crystalline product had formed. Neutron powder diffraction data were collected using the D2b diffractometer at the ILL, Grenoble, $\lambda = 1.59378(3)$ Å (the wavelength was calibrated against X-ray data). Diffraction experiments were carried out at 290, 20, and 2 K. The diffractometer D1b at ILL, $\lambda = 2.5192$ Å, was used to record the evolution of the diffraction pattern as a function of temperature. Data were collected between 2 and 60 K with a ramp rate of 6.75 K h^{-1} and a counting time of 20 min, thus generating a set of diffraction patterns with a temperature resolution of 2.5 K. Rietveld analyses of both X-ray and neutron diffraction data were performed using the GSAS program suite.[21]

Magic-angle-spinning (MAS) solid-state nuclear magnetic resonance experiments were performed using a CMX200 spectrometer at an operating frequency of 77.79 MHz for ^7Li, with $\pi/2$ pulse lengths of 2.8 μs and a spinning speed of 30 kHz.

Electron diffraction patterns and high-resolution lattice images were recorded on JEOL 4000EX, 3000F, and 2000FX transmission

(8) Argyriou, D. N.; Bordallo, H. N.; Campbell, B. J.; Cheetham, A. K.; Cox, D. E.; Gardner, J. S.; Hanif, K.; dos Santos, A.; Strouse, G. F. *Phys. Rev. B* **2000**, *61*, 15269.
(9) Battle, P. D.; Millburn, J. E.; Rosseinsky, M. J.; Spring, L. E.; Vente, J. F.; Radaelli, P. G. *Chem. Mater.* **1997**, *9*, 3136.
(10) Green, M. A.; Neumann, D. A. *Chem. Mater.* **2000**, *12*, 90.
(11) Demazeau, G.; Ohkim, E. O.; Wang, K. T.; Fournes, L.; Dance, J. M.; Pouchard, M.; Hagenmuller, P. *Rev. Chim. Mineral.* **1987**, *24*, 183.
(12) Attfield, J. P.; Ferey, G. *J. Solid State Chem.* **1989**, *80*, 112.
(13) Demazeau, G.; Pouchard, M.; Zhu, J. L.; Hagenmuller, P. *Z. Anorg. Allg. Chem.* **1988**, *555*, 64.
(14) Villeneuve, G.; Rojo, T.; Demazeau, G.; Hagenmuller, P. *Mater. Res. Bull.* **1988**, *23*, 1787.
(15) Abou-Warda, S.; Pietzuch, W.; Berghofer, G.; Kesper, U.; Massa, W.; Reinen, D. *J. Solid State Chem.* **1998**, *138*, 18.
(16) Warda, S. A.; Massa, W.; Reinen, D.; Hu, Z. W.; Kaindl, G.; de Groot, F. M. F. *J. Solid State Chem.* **1999**, *146*, 79.
(17) Abbattista, F.; Vallino, M.; Mazza, D. *J. Less-Common Met.* **1985**, *110*, 391.
(18) Battle, P. D.; Green, M. A.; Laskey, N. S.; Millburn, J. E.; Murphy, L.; Rosseinsky, M. J.; Sullivan, S. P.; Vente, J. F. *Chem. Mater.* **1997**, *9*, 552.
(19) Caldes, M.; Michel, C.; Rouillon, T.; Hervieu, M.; Raveau, B. *J. Mater. Chem.* **2002**, *12*, 473.
(20) Kamegashira, N.; Meng, J.; Mori, T.; Murase, A.; Satoh, H.; Shishido, T.; Fukuda, T. *Mater. Lett.* **2003**, *57*, 1941.
(21) Larson, A. C.; von Dreele, R. B. *General Structure Analysis System (GSAS)*; Report LAUR 86-748; Los Alamos National Laboratories: Los Alamos, NM, 1990.

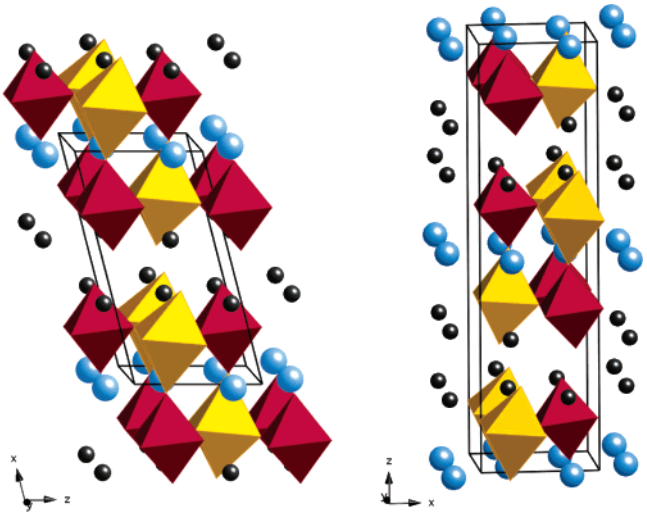

Figure 1. Crystal structure of $Nd_2BaLiRuO_7$ described in (a) space group $P2_1$ and (b) space group $B2_1$. RuO_6 and LiO_6 octahedra are colored red and yellow, respectively. Large blue and small black circles represent Ba and Nd, respectively.

electron microscopes (TEM) operated at 400, 300, and 200 kV, respectively. Image simulations based on the structural data determined in X-ray and neutron diffraction experiments were performed using the Java EMS software package; C_s values of 0.6 and 1.0 mm were used for the simulation of images obtained on the 3000F and 4000EX, respectively.

Magnetometry experiments were carried out using a Quantum Design MPMS SQUID magnetometer. Magnetic susceptibilities were recorded in a field of 100 Oe after cooling in both zero field (zfc) and in the measuring field (fc). Hysteresis measurements were made at a constant temperature in the field range $-50 \leq H/\text{kOe} \leq +50$ after cooling from room temperature in a field of +50 kOe.

Results

Structural Chemistry of $Nd_2BaLiRuO_7$. The fwhm of the reflections in the X-ray powder diffraction pattern of the reaction product showed that the sample was highly crystalline. Bragg peaks were observed in both the neutron and X-ray powder diffraction data that could not be accounted for in the ideal $n = 2$ RP space group $I4/mmm$ or in the space group $P4_2/mnm$, which allows for some rotation of the B-site octahedra. These superlattice reflections were found to be consistent with cation ordering over the B sites. A model of 1:1 cation ordering that required a lowering of the crystal symmetry from body-centered tetragonal to primitive monoclinic, space group $P2_1$ (No. 4), was devised. Simultaneous analysis of X-ray and neutron diffraction data could be successfully carried out using this structural model, with a unit cell of 10.6053(2) × 5.56889(8) × 5.60315(8) Å, $\beta = 105.378(1)°$, $V = 319.07(1)$ Å^3. The volume of this unit cell (Figure 1a) is close to that of the usual (~3.8 × 3.8 × 20 Å) $n = 2$ unit cell. However, although there were no additional peaks in either the X-ray or the neutron data to indicate that this model was incorrect, additional spots clearly present along c^* in electron diffraction patterns (Figure 2) could only be indexed in a larger unit cell (~5.5 × ~5.5 × ~20 Å, $\beta \sim 90°$) in space group $P2_1$ (Figure 1b).

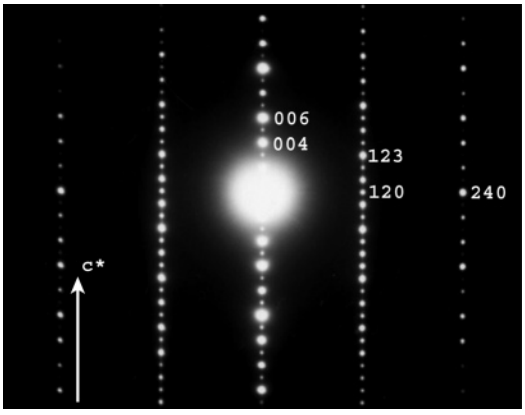

Figure 2. Electron diffraction pattern of $Nd_2BaLiRuO_7$ viewed along $[2\bar{1}0]$ zone axis of a unit cell with $a = 5.60328(7)$ Å, $b = 5.56901(6)$ Å, $c = 20.4518(3)$ Å, $V = 638.19(1)$ Å^3. The pattern was taken using a 2000FX TEM.

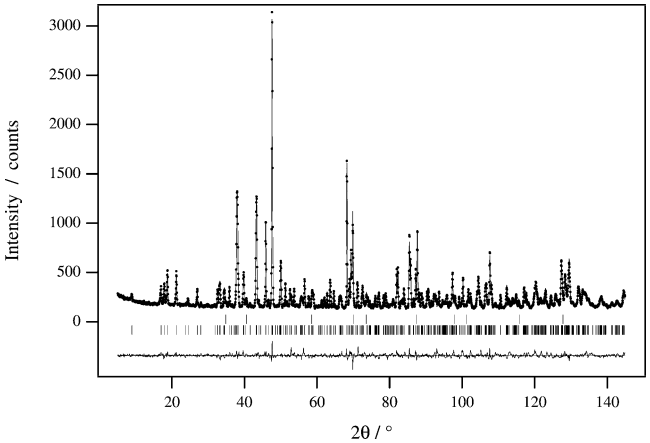

Figure 3. Observed (●), calculated (—), and difference neutron diffraction profiles for $Nd_2BaLiRuO_7$ at room temperature. The upper set of tick marks indicates the positions of reflections attributable to the minority phase, Li_2O, and the lower set relates to $Nd_2BaLiRuO_7$.

The unit cell vectors of the two settings are related as follows: $\mathbf{a}' = \mathbf{c}$, $\mathbf{b}' = -\mathbf{b}$, and $\mathbf{c}' = 2\mathbf{a} + \mathbf{c}$.

For ease of comparison, the final analysis of the X-ray and neutron diffraction data was carried out in a unit cell ~5.5 × ~5.5 × ~20 Å, despite the fact that they could be accounted for using a unit cell of half the volume. The structure was constrained to that refined in the smaller, primitive cell by the use of the nonstandard space group setting $B2_1$ to describe the larger cell. Thus, all our diffraction data are described in comparable unit cells, although the structural feature responsible for the $00l$, $l = 2n + 1$ superlattice reflections seen in Figure 2 remains unidentified and is therefore not modeled in the X-ray and neutron data analysis. Combined refinements against neutron and X-ray powder data were carried out to optimize our structural model of $Nd_2BaLiRuO_7$. Trial refinements found no evidence of vacancies on the oxygen sites and these sites were subsequently constrained to be fully occupied. The degree of Li/Ru ordering was allowed to vary. Ordering on the A site was also included in the refinements and resulted in complete occupation by Nd of the 9-coordinate sites in the rock-salt layer and by Ba of the 12-coordinate sites within the perovskite layer. The A sites were therefore constrained to be fully ordered in the final refinements. To define the origin

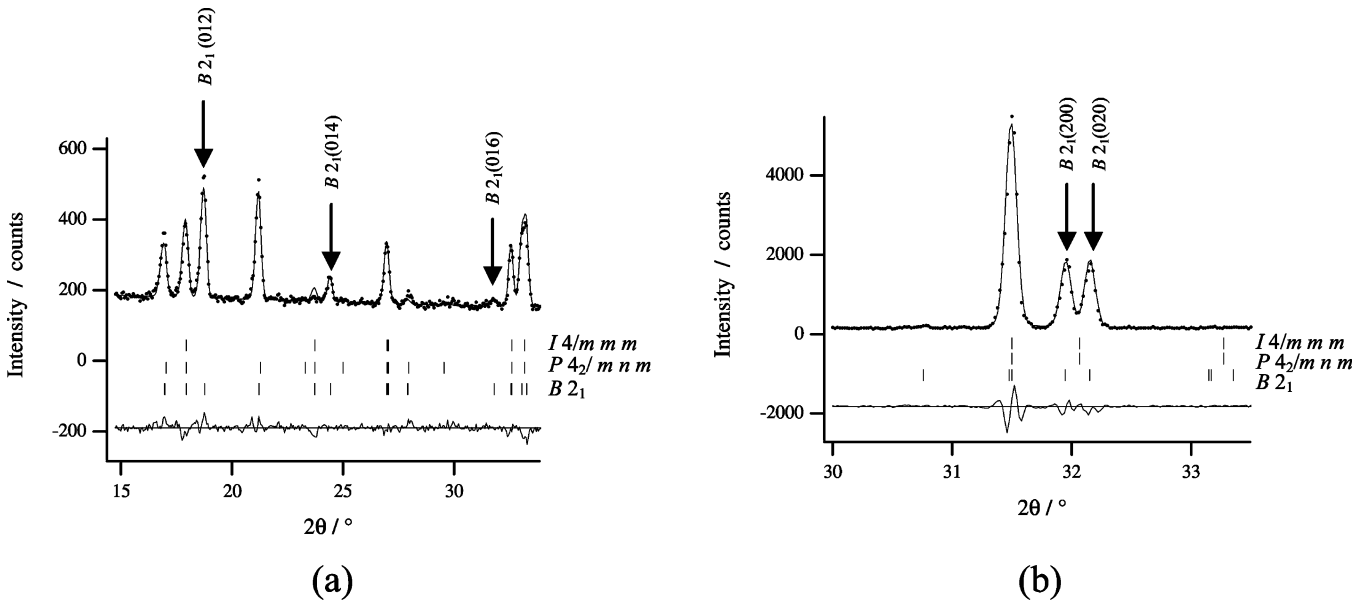

Figure 4. Enlarged angular regions (a) $15 \leq 2\theta/° \leq 34$ of the neutron diffraction profile and (b) $31 \leq 2\theta° \leq 34$ of the X-ray diffraction profile for $Nd_2BaLiRuO_7$; allowed reflection positions are shown by tick marks for space groups $I4/mmm$, $P4_2/mnm$, and $B2_1$.

Table 1. Atomic Coordinates for $Nd_2BaLiRuO_7$ at Room Temperature from Combined Analysis of X-ray and Neutron Diffraction Data[a]

atom	*x*	*y*	*z*	U_{iso} (Å^2)	occupancy
Ba	0.7461(9)	0.75	0.0003(2)	0.0046(7)	1
Nd1	0.7208(7)	0.748(2)	0.1814(1)	0.0085(7)	1
Nd2	0.2600(8)	0.269(2)	0.1826(1)	0.0060(7)	1
Li/Ru1	0.226(3)	0.730(3)	0.0974(8)	0.0022(6)	0.964(4)
Li/Ru2	0.749(1)	0.263(2)	0.1020(1)	0.0022(6)	0.036(4)
O1	0.2242(9)	0.765(2)	0.9885(2)	0.0098(4)	1
O2	0.507(2)	0.512(2)	0.1016(6)	0.0098(4)	1
O3	0.995(2)	0.505(2)	0.1138(4)	0.0098(4)	1
O4	0.7118(9)	0.250(2)	0.2050(2)	0.0098(4)	1
O5	0.995(2)	0.018(2)	0.1195(4)	0.0098(4)	1
O6	0.3154(9)	0.701(2)	0.2118(3)	0.0098(4)	1
O7	0.506(2)	0.010(2)	0.1025(6)	0.0098(4)	1

[a] Space group $B2_1$; $a = 5.60328(7)$ Å, $b = 5.56901(6)$ Å, $c = 20.4518(3)$ Å, $\beta = 90.061(1)°$. The fractional occupancies of the B-sites refer to the proportion of Li occupying the site. Weight percent of $Li_2O = 0.70(5)\%$. Goodness of fit parameters of $\chi^2 = 2.583$, X-ray $R_{wp} = 9.16$, $R_p = 7.19$, neutron $R_{wp} = 6.30$, $R_p = 4.66$, overall $R_{wp} = 7.15$, $R_p = 6.26$, 86 variables.

of the unit cell, the *y* coordinate of the Ba atom was fixed at 0.75. All atomic thermal parameters were constrained to be isotropic and 41 atomic parameters were varied in the final refinement. Although not detected in the X-ray diffraction patterns, inspection of the neutron diffraction pattern revealed a small excess of lithium oxide to be present in the sample. The results of the refinement against the neutron data are presented in Figure 3 and those sections of the diffraction profiles that were crucial in identifying the distortion from tetragonal symmetry are shown in Figure 4. The lattice parameters and atomic coordinates are listed in Table 1, and selected bond distances and angles are shown in Table 2. The atom labeling scheme used in the tables is explained in Figure 5, which also serves to illustrate the local environment around each cation.

The ^{7}Li MAS NMR spectrum of $Nd_2BaLiRuO_7$, shown in Figure 6, consists of a single resonance, with a hyperfine shift of −14 ppm, accompanied by spinning sidebands and thus indicates that there is only one local environment for lithium in this compound.

Table 2. Selected Bond Distances (Å) and Angles (°) in $Nd_2BaLiRuO_7$ at Room Temperature

Ba−O1	2.936(6)	Nd2−O5	2.41(1)
Ba−O1	2.691(7)	Nd2−O6	3.234(6)
Ba−O1	2.71(1)	Nd2−O6	2.498(7)
Ba−O1	2.88(1)	Nd2−O6	2.233(6)
Ba−O2	2.80(1)	Nd2−O7	2.58(1)
Ba−O2	2.91(1)	mean Nd−O	2.6(3)
Ba−O3	3.03(1)		
Ba−O3	3.10(1)	Li−O1	2.28(2)
Ba−O5	3.18(1)	Li−O2	1.99(2)
Ba−O5	3.13(1)	Li−O3	1.83(2)
Ba−O7	2.88(1)	Li−O5	2.11(2)
Ba−O7	2.86(2)	Li−O6	2.40(2)
mean Ba−O	2.9(1)	Li−O7	2.21(2)
		mean Li−O	2.1(2)
Nd1−O2	2.41(1)		
Nd1−O3	2.47(1)	Ru−O1	1.857(5)
Nd1−O4	2.817(8)	Ru−O2	1.94(1)
Nd1−O4	2.835(8)	Ru−O3	1.94(1)
Nd1−O4	2.354(5)	Ru−O4	2.117(5)
Nd1−O5	2.50(1)	Ru−O5	1.97(1)
Nd1−O6	2.370(7)	Ru−O7	1.96(1)
Nd1−O6	3.399(7)	mean Ru−O	1.96(8)
Nd1−O7	2.48(1)		
		Li−O1−Ru	172.6(7)
Nd2−O2	2.55(1)	Li−O2−Ru	171.6(7)
Nd2−O3	2.43(1)	Li−O3−Ru	162.3(8)
Nd2−O4	3.108(6)	Li−O5−Ru	156.4(7)
Nd2−O4	2.574(6)	Li−O7−Ru	176.8(9)

Electron diffraction patterns and images were taken along a selection of zone axes for $Nd_2BaLiRuO_7$. The [100], [110], and [2$\bar{1}$0] diffraction patterns all showed additional reflections along c^* that could not be indexed in the smaller (V (Å^3) = 319.07(1)) cell suggested by the neutron and X-ray diffraction data. The patterns could only be indexed in a larger pseudo-tetragonal unit cell of volume 638.19(1) Å^3. A selected-area electron diffraction pattern (Figure 7), a high-resolution lattice image (Figure 8), and a focal series (Figure 9) were collected for the [100] zone. Those reflections forbidden in space group $P2_1$ that are present in the diffraction pattern can be ascribed to double diffraction. The correct assignment of the zone axis was confirmed by the B-site ordering observed in the lattice image, and by the

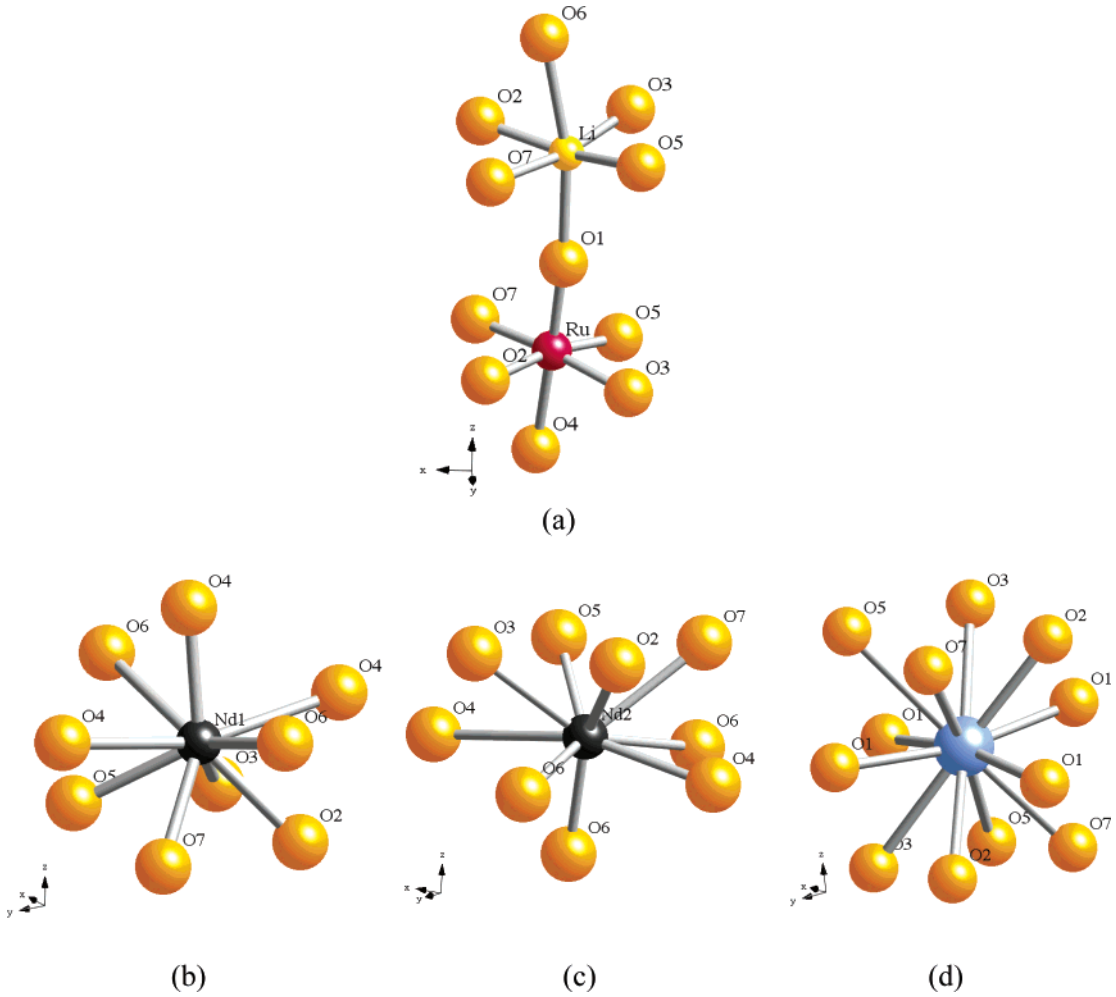

Figure 5. Arrangement of the oxygen atoms surrounding the (a) B-site cations, (b) Nd1 cations, (c) Nd2 cations, and (d) Ba cations within $Nd_2BaLiRuO_7$.

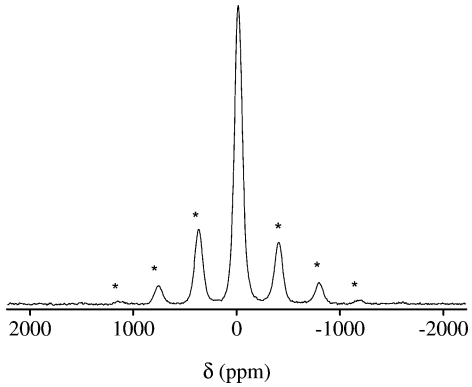

Figure 6. Magnetic-angle-spinning ^7Li NMR spectrum of $Nd_2BaLiRuO_7$, acquired with a spinning speed of 30 kHz. Spinning sidebands (*) are indicated.

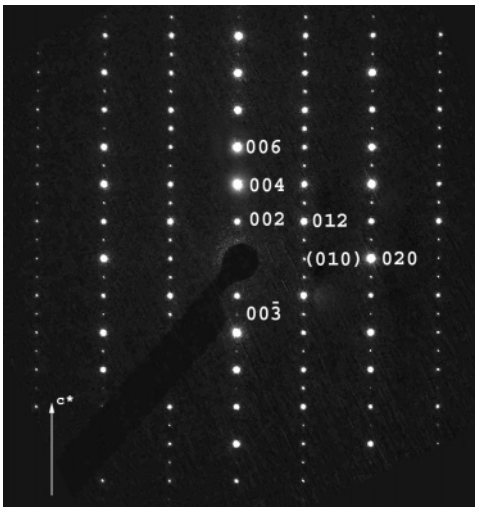

Figure 7. Selected area electron diffraction pattern of [100] zone axis of $Nd_2BaLiRuO_7$; 0*k*0, *k* odd reflections, e.g., (010), result from double diffraction.

agreement between the observed and calculated images in the focal series. The stacking faults that were observed[4] in [100] images of La_3LiMnO_7 are not apparent in the present case. Figure 10 shows the selected area diffraction pattern and lattice images of the [110] zone indexed in the space group $P2_1$. The [110] zone is insensitive to the long-range B-site ordering present within the perovskite layers but clearly shows the additional reflections along *c** that could not be indexed in the smaller unit cell. A diffraction pattern and lattice images recorded for the [001] zone at different defoci are presented in Figure 11. A high degree of structural coherence is again apparent.

Magnetic Properties of $Nd_2BaLiRuO_7$. The magnetic susceptibility of $Nd_2BaLiRuO_7$ (Figure 12) increases slowly on cooling with a local plateau occurring at 40(2) K, a point of inflection at 32(2) K, and a global maximum at 8(2) K. The data were fitted using the Curie−Weiss law over the

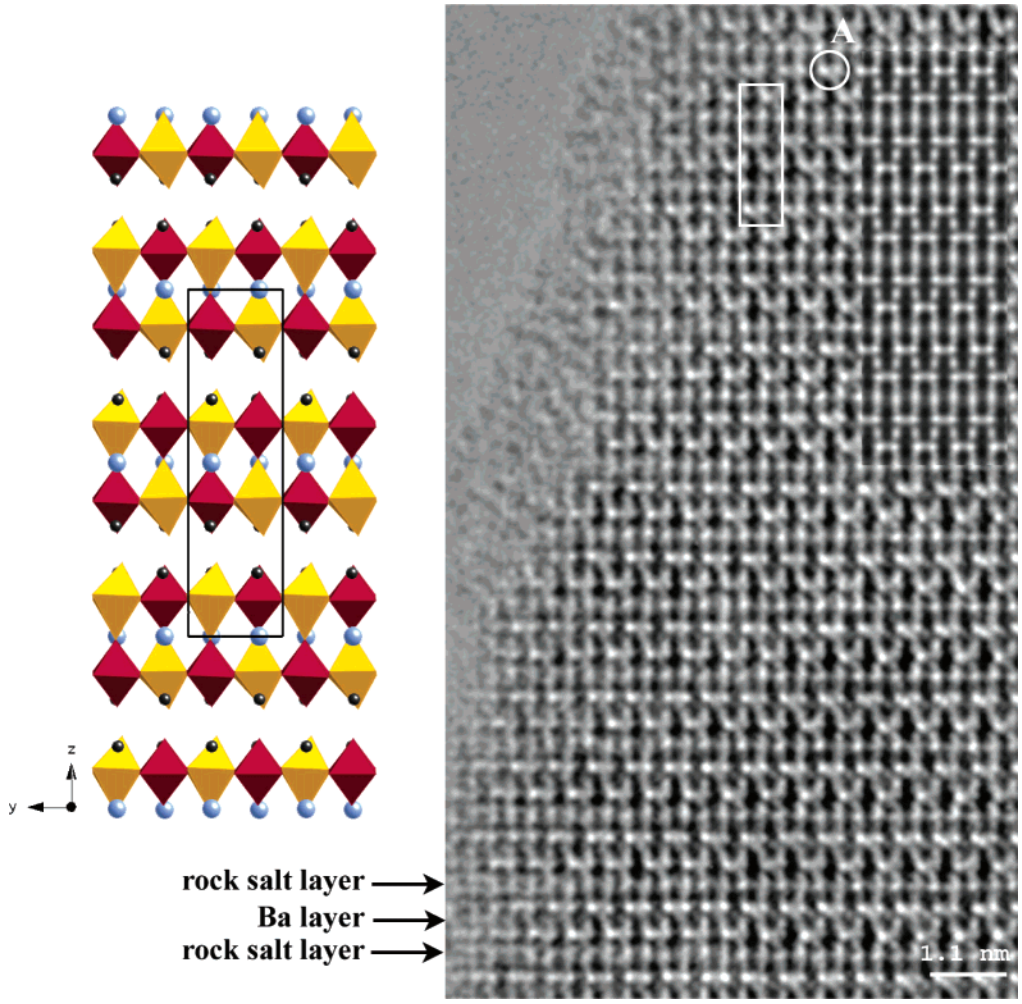

Figure 8. High-resolution electron image of $Nd_2BaLiRuO_7$, [100] projection, showing the long-range ordering of lithium and ruthenium present within the crystal. The regions of light contrast (e.g., A) can be taken to represent the position of the lithium atom. The simulation on the right of the image is at defocus 20 nm and crystal thickness of 3.9 nm. A white rectangle on the upper center part of the lattice image represents a unit cell of the crystal, with a pictorial representation of the [100] projection to the left of the image.

temperature range $65 \leq T/\mathrm{K} \leq 300$, where the zero-field-cooled (zfc) and field-cooled (fc) data sets overlie, giving values for the Curie constant $C = 5.14(2)$ cm^3 mol^{-1} K^{-1} and Weiss constant $\theta = -50.3(6)$ K. The field dependence of the magnetization was investigated at 5, 20, and 150 K (Figure 13) and no significant hysteresis was observed at any temperature.

The majority of the reflections present in the neutron diffraction data collected at 2 and 20 K from $Nd_2BaLiRuO_7$ could be accounted for by the room-temperature structural model. However, a number of additional high *d*-spacing reflections were observed in both sets of low-temperature data, suggestive of the presence of long-range magnetic order. The magnetic Bragg peaks could be indexed using a $2a \times 2b \times c$ expansion of the structural unit cell. During the analysis of these data, the occupancies of the B-site cations and the fraction of the impurity phase, Li_2O, were held fixed at the values obtained from the refinement against the diffraction data collected at room temperature. A number of trial refinements were undertaken employing the 20 K data set. Stable refinements were obtained when the magnetic scattering was assumed to come entirely from Ru^{5+}. This was consistent with the magnetometry data that indicated the presence of a transition at 32(2) K before the global maximum at 8(2) K. A number of suitable models were tested against the data. Figure 14 shows the diffraction profiles resulting from the most successful model, which is drawn in Figure 15 and described in Table 3. The crystal structure did not change significantly on cooling; the unit cell parameters at 20 K refined to the following values: space group $B2_1$; $a = 5.5927(1)$ Å, $b = 5.5605(1)$ Å, $c = 20.3942(5)$ Å, $\beta = 90.032(3)°$. The NN spins within a single perovskite sheet (a pseudo-square lattice) are ordered antiferromagnetically, thus causing the doubling of the magnetic cell in the *xy* plane. There are two plausible ways, resulting in equal amounts of magnetic frustration, of coupling the antiferromagnetic ruthenium layers within the individual $n = 2$ perovskite blocks. Both types of order exist within the model and occur alternately on passing from block to block along the *z* axis, as shown in Figure 15. The difference in the stacking can be seen by examining the spins within a perovskite sheet and comparing their direction (up/down) with that of the spins in the other sheet of the same block. In the [110] view of the bilayer centered on $z = 0$, each spin is aligned antiparallel with those above or below it in the same block. In the layer centered on $z = {}^1/_2$, each spin is aligned parallel with that above or below it in the [110] view; the description is reversed if the structure is viewed

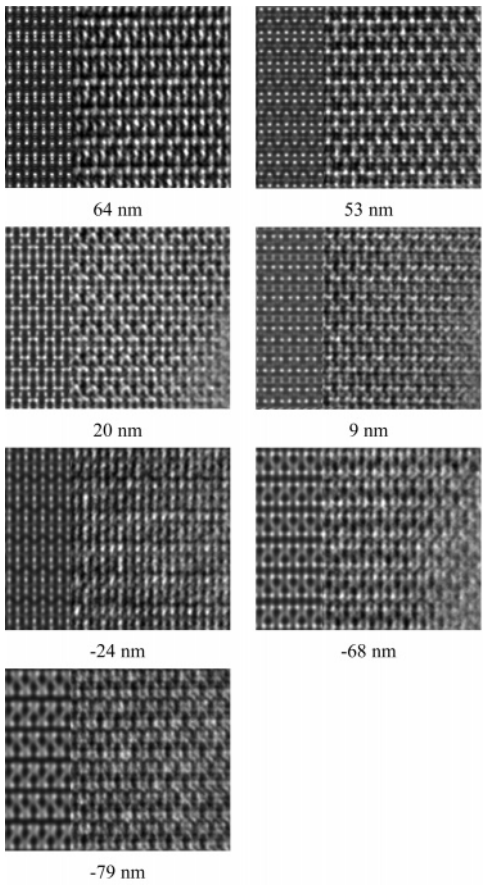

Figure 9. Through focal series of images of $Nd_2BaLiRuO_7$ in the [100] projection, defocus values for simulated images (left of each frame), calculated for a crystal thickness of 3.9 nm, are given below the images.

along [$1\bar{1}0$]. The two plausible intrablock coupling schemes thus occur with equal weight.

Constraining the ordered components of the magnetic moment to lie along the unique axis, *y*, did not result in a successful refinement and consequently all magnetic components were refined. The net moment of Ru^{5+} was refined to have a magnitude of 2.1(2) μ_B with the components along the crystallographic axes of $m_x = 1.6(4)\ \mu_B$, $m_y = 1.0(5)\ \mu_B$, and $m_z = 1.1(3)\ \mu_B$. The large standard deviation on all magnetic components is a result of the low ratio of observed magnetic peaks to variable vector components.

Cooling to 2 K resulted in a strong increase in all the magnetic peaks that were observed at 20 K and an increase in the intensity of the partially magnetic 113 reflection. Trial refinements using the $2a \times 2b \times c$ expansion of the structural unit cell included magnetic moments on both Ru and Nd. A number of magnetic models were investigated and the most suitable model for the 2 K data is shown in Figure 16. This magnetic structure can be described as a herringbone-type alignment of the spins on both Ru and Nd, predominately along the *z* axis. The net moment of Nd^{3+} was refined to have a magnitude of 2.53(8) μ_B, with the components $m_x = 1.8(1)\ \mu_B$, $m_y = 0.4(1)\ \mu_B$, and $m_z = 1.7(1)\ \mu_B$. The ruthenium moment refined to a net value of 2.2(2) μ_B, the components along the crystallographic axes being $m_x = 1.3(2)\ \mu_B$, $m_y = 0.0(3)\ \mu_B$, and $m_z = 1.7(1)\ \mu_B$. The structural unit cell parameters refined to the values $a = 5.5929(1)$ Å, $b = 5.5604(1)$ Å, $c = 20.3954(5)$ Å, $\beta = 90.024(3)°$. The diffraction profiles are presented in Figure 17 and the atomic coordinates and moments of the Nd and Ru cations are detailed in Table 4.

Neutron powder diffraction data were also collected on D1b, ILL, between 2 and 60 K, with a temperature resolution of 2.5 K. The evolution of the diffraction pattern with decreasing temperature showed the onset of magnetic peaks at approximately 33.25(±1.25) K and is presented in Figure 18. The temperature dependence of the intensity of several individual peaks was measured and these results are presented in Figure 19. The intensity of the structural (S) reflection 012, which has a very low magnetic (M) contribution, remains approximately constant in intensity over the temperature range. However, the other reflections that were selected for investigation all increased in intensity with decreasing temperature due to the ordering of the magnetic moments of the Ru and Nd cations. All reflections with a magnetic component initially increase gradually with decreasing temperature, but below approximately 20 K there is a more rapid increase in intensity with decreasing in temperature. The 111 (M) and 112 (M) both appear in the diffraction pattern at approximately 33.25 (± 1.25) K and show a gradual increase in intensity with decreasing temperature, but with a sharper gradient between approximately 20 and 10 K, before leveling off after 10 K. In contrast, the 113 (M) reflection, which has a structural component, and the 110 (M), which is a purely magnetic reflection, both increase in intensity down to 2 K and it was found, by varying the contribution of the neodymium and ruthenium moments in trial calculations, that these reflections contained a stronger neodymium component than the 111 (M) and 112

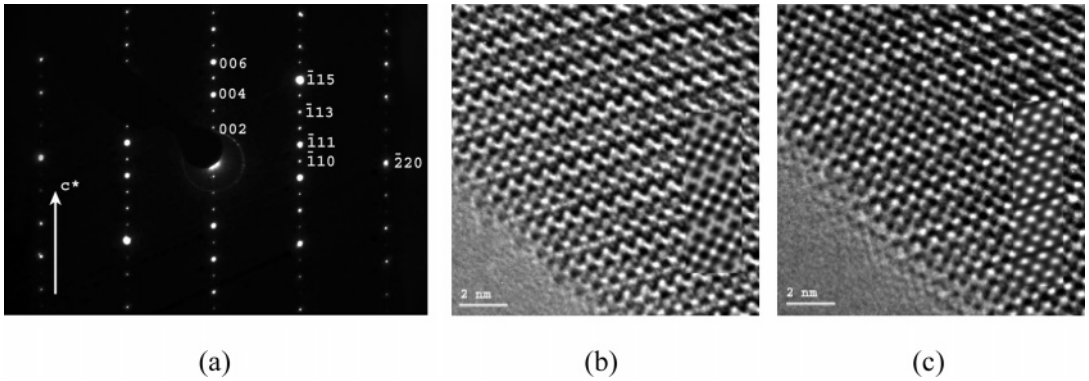

Figure 10. The [110] zone axis of $Nd_2BaLiRuO_7$: (a) selected area electron diffraction, (b) lattice image with simulation (right) at defocus −10 nm and crystal thickness 3.1 nm and (c) lattice image with simulation (right) at defocus −70 nm and crystal thickness 3.1 nm.

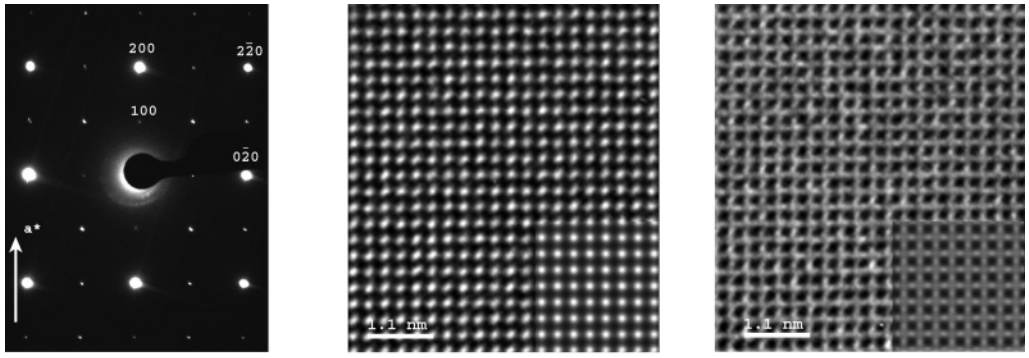

Figure 11. The [001] zone axis of $Nd_2BaLiRuO_7$: (a) selected area electron diffraction, (b) lattice image with simulation (bottom right) at defocus 20 nm and crystal thickness 2 nm and (c) lattice image with simulation (bottom right) at defocus 30 nm and crystal thickness 2 nm.

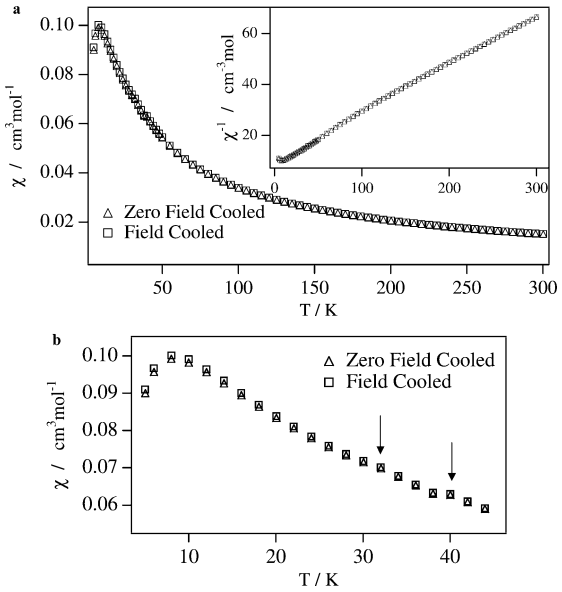

Figure 12. (a) Temperature dependence of the molar magnetic susceptibility and (inset) reciprocal molar susceptibility of $Nd_2BaLiRuO_7$ in an applied field of 100 Oe. (b) Detail of temperature dependence of molar magnetic susceptibility, with changes in gradient arrowed.

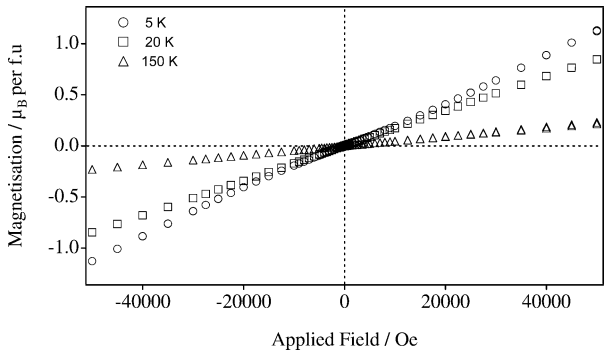

Figure 13. Field dependence of the magnetization of $Nd_2BaLiRuO_7$ at 5, 20, and 150 K.

(M) peaks. This is consistent with our interpretation of the susceptibility data in that the changes below 10 K are primarily attributable to the onset of long-range antiferromagnetic order on the Nd sublattice.

Discussion

The results presented above extend both the range of known Ba-containing $n = 2$ RP phases and the number of these phases in which cation ordering has been observed. Among the few Ba-containing $n = 2$ RP phases that have been investigated previously are $Ln_2BaIn_2O_7$ (Ln = La, Nd)[19] and $Gd_2BaMn_2O_7$.[20] These compounds exhibit complete A-site ordering of the type observed in $Nd_2BaLiRuO_7$, with the larger barium ion occupying the 12-coordinate sites within the perovskite blocks and the rare-earth occupying the 9-coordinate sites on the boundaries of the blocks. This type of A-site ordering has also been observed in Sr containing $n = 2$ RP phases (e.g., $Sr_2HoMn_2O_7$[9]). However, $Nd_2BaLiRuO_7$ is the first $n = 2$ RP phase in which simultaneous ordering of the A and B sites has been observed. Within the $Nd_2BaLiRuO_7$ structure the Nd cations and oxide anions are displaced from their ideal sites and a marked distortion of the NdO layers is observed. The distortion is more marked than that observed in $Ln_2BaIn_2O_7$, which was described as an islandlike configuration (Figure 20) of the A-site cations.[19] This change in distortion must be a result of the difference in the tilting of the ordered BO_6 octahedra observed in $Nd_2BaLiRuO_7$ compared to that seen in $Ln_2BaIn_2O_7$ where no cation order is present on the B sites.

The type of long-range B-site ordering observed in $Nd_2BaLiRuO_7$ is that which was proposed by Burley et al. for La_3LiMnO_7, which exhibited 1:1 ordering over a much

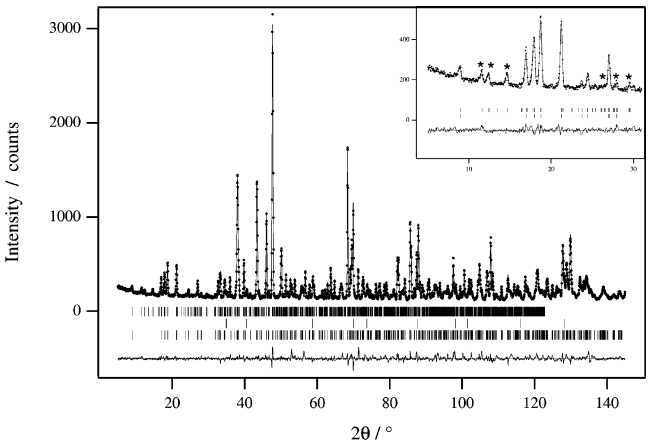

Figure 14. Observed (●), calculated (—), and difference neutron diffraction profiles for $Nd_2BaLiRuO_7$ at 20 K. Tick marks indicate reflection positions for (descending order) the magnetic phase, the minority phase (Li_2O), and $Nd_2BaLiRuO_7$. Magnetic reflections are highlighted (*) in the inset. $\chi^2 = 6.138$, $R_{wp} = 7.30$, $R_p = 5.28$, 67 variables.

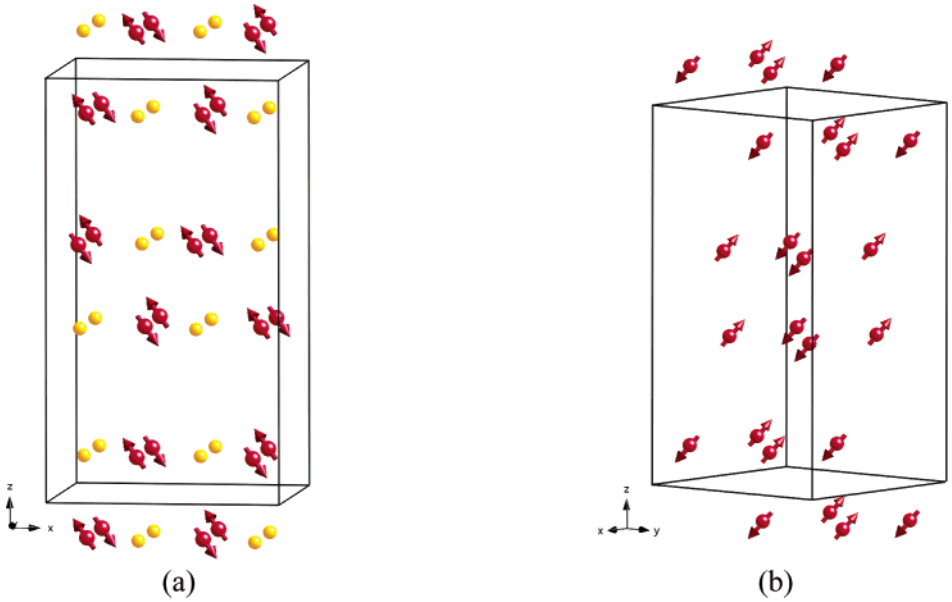

Figure 15. Magnetic structure of $Nd_2BaLiRuO_7$ at 20 K: arrows represent the relative spin direction of the Ru moment. (a) View with Li atoms are shown for clarity; (b) [110] view to show the alternating ordering of the Ru moments in neighboring bilayers.

Table 3. Atomic Coordinates and Ordered Moments of Ruthenium Atoms within the Magnetic Structure of $Nd_2BaLiRuO_7$ at 20 K

atom[a]	*x*	*y*	*z*	m_x/μ_B	m_y/μ_B	m_z/μ_B
Ru1	0.3724(8)	0.132(2)	0.1014(2)	−1.6(4)	1.0(5)	1.1(3)
Ru2	0.8724(8)	0.132(2)	0.1014(2)	1.6(4)	−1.0(5)	−1.1(3)
Ru3	0.1276(8)	0.382(2)	0.8984(2)	−1.6(4)	1.0(5)	1.1(3)
Ru4	0.6276(8)	0.382(2)	0.8984(2)	1.6(4)	−1.0(5)	−1.1(3)
Ru5	0.1224(8)	−0.132(2)	0.6014(2)	1.6(4)	−1.0(5)	−1.1(3)
Ru6	0.6224(8)	−0.132(2)	0.6014(2)	−1.6(4)	1.0(5)	1.1(3)
Ru7	0.3776(8)	0.382(2)	0.3984(2)	1.6(4)	−1.0(5)	−1.1(3)
Ru8	0.8776(8)	0.382(2)	0.3984(2)	−1.6(4)	1.0(5)	1.1(3)

[a] Each atom is reproduced at $(x, y, z) + (1/2, 1/2, 0)$.

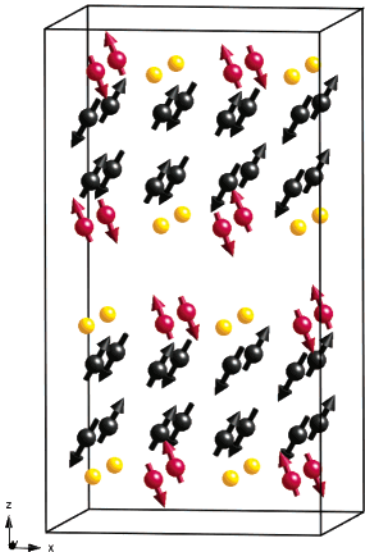

Figure 16. Magnetic structure of $Nd_2BaLiRuO_7$ at 2 K. Magnetic Nd and Ru atoms are represented by black and red circles; nonmagnetic Li atoms by yellow circles.

shorter length scale. The greater charge difference between Li^+ and Ru^{5+} provides enough contrast between the B-site cations to induce long-range order in the current phase. Consequently, this leads to a lowering of the crystal symmetry, from body-centered tetragonal (*I4/mmm*) to primitive monoclinic ($P2_1$). However, as we shall emphasize

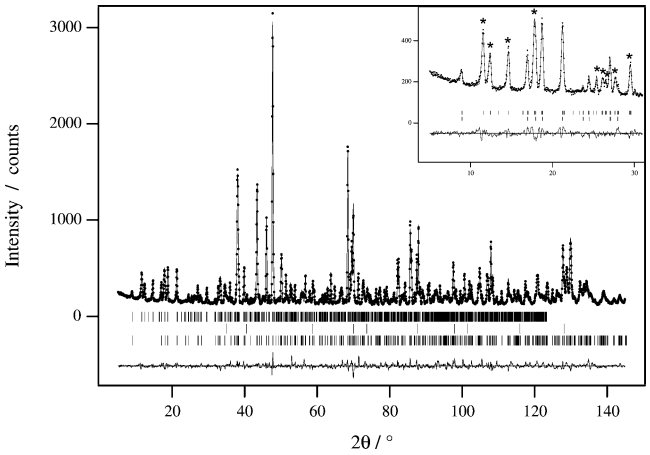

Figure 17. Observed (●), calculated (—), and difference neutron diffraction profiles for $Nd_2BaLiRuO_7$ at 2 K. Tick marks indicate reflection positions for (descending order) the magnetic phase, the minority phase (Li_2O), and $Nd_2BaLiRuO_7$. Magnetic reflections are highlighted (*) in the inset. $\chi^2 = 6.415$, $R_{wp} = 7.45$, $R_p = 5.47$, 68 variables.

below, our electron diffraction patterns demonstrate that our neutron diffraction data do not reveal the full details of the microstructure adopted by $Nd_2BaLiRuO_7$. The relatively small spread of Ru−O bond distances resulting in almost regular RuO_6 octahedra is typical of Ru(V) oxides, and the values in Table 2 are similar to those observed in other Ru(V) perovskite-related materials.[5,22−27] However, in contrast to the RuO_6 octahedra, significant distortion of the LiO_6 octahedra was observed. Although the mean length of the Li−O bonds is comparable with published values for related

(22) Battle, P. D.; Jones, C. W. *J. Solid State Chem.* **1989**, *78*, 108.
(23) Battle, P. D.; Goodenough, J. B.; Price, R. *J. Solid State Chem.* **1983**, *46*, 234.
(24) Battle, P. D.; Jones, C. W.; Studer, F. *J. Solid State Chem.* **1991**, *90*, 302.
(25) Shaked, H.; Jorgenson, J. D.; Chmaissem, O.; Ikeda, S.; Maeno, Y. *J. Solid State Chem.* **2000**, *154*, 361.
(26) Hong, K. P.; Choi, Y. H.; Kwon, Y. U.; Jung, D. Y.; Lee, J. S.; Shim, H. S.; Lee, C. H. *J. Solid State Chem.* **2000**, *150*, 383.
(27) Izumiyama, Y.; Doi, Y.; Wakeshima, M.; Hinatsu, Y.; Oikawa, K.; Shimojo, Y.; Morii, Y. *J. Mater. Chem.* **2000**, *10*, 2364.

Table 4. Atomic Coordinates and Ordered Magnetic Moments of Ru and Nd Atoms within the Magnetic Structure of $Nd_2BaLiRuO_7$ at 2 K

atom[a]	*x*	*y*	*z*	m_x/μ_B	m_y/μ_B	m_z/μ_B
Ru1	0.3730(8)	0.132(2)	0.1016(2)	1.3(2)	−0.0(3)	−1.8(1)
Ru2	0.8730(8)	0.132(2)	0.1016(2)	−1.3(2)	0.0(3)	1.8(1)
Ru3	0.1270(8)	0.382(2)	0.8984(2)	1.3(2)	−0.0(3)	−1.8(1)
Ru4	0.6270(8)	0.382(2)	0.8984(2)	−1.3(2)	0.0(3)	1.8(1)
Ru5	0.1230(8)	0.132(2)	0.6016(2)	−1.3(2)	0.0(3)	1.8(1)
Ru6	0.6230(8)	0.132(2)	0.6016(2)	1.3(2)	−0.0(3)	−1.8(1)
Ru7	0.3770(8)	0.382(2)	0.3984(2)	−1.3(2)	0.0(3)	1.8(1)
Ru8	0.8770(8)	0.382(2)	0.3984(2)	1.3(2)	−0.0(3)	−1.8(1)
Nd1	0.3600(6)	0.376(1)	0.1812(2)	1.8(1)	−0.4(1)	1.7(1)
Nd2	0.8600(6)	0.376(1)	0.1812(2)	−1.8(1)	0.4(1)	−1.7(1)
Nd3	0.1403(6)	0.126(1)	0.8187(2)	−1.8(1)	0.4(1)	−1.7(1)
Nd4	0.6403(6)	0.126(1)	0.8187(2)	1.8(1)	−0.4(1)	1.7(1)
Nd5	0.1100(6)	0.376(1)	0.6813(3)	1.8(1)	−0.4(1)	1.7(1)
Nd6	0.6100(6)	0.376(1)	0.6813(3)	−1.8(1)	0.4(1)	−1.7(1)
Nd7	0.3900(6)	0.126(1)	0.3187(2)	1.8(1)	−0.4(1)	1.7(1)
Nd8	0.8900(6)	0.126(1)	0.3187(2)	−1.8(1)	0.4(1)	−1.7(1)
Nd9	0.1309(6)	0.133(1)	0.1826(2)	−1.8(1)	0.4(1)	−1.7(1)
Nd10	0.6309(6)	0.133(1)	0.1826(2)	1.8(1)	−0.4(1)	1.7(1)
Nd11	0.3690(6)	0.383(1)	0.8174(2)	1.8(1)	−0.4(1)	1.7(1)
Nd12	0.8690(6)	0.383(1)	0.8174(2)	−1.8(1)	0.4(1)	−1.7(1)
Nd13	0.3810(6)	0.133(1)	0.6826(2)	1.8(1)	−0.4(1)	1.7(1)
Nd14	0.8810(6)	0.133(1)	0.6826(2)	−1.8(1)	0.4(1)	−1.7(1)
Nd15	0.1190(6)	0.383(1)	0.3174(2)	1.8(1)	−0.4(1)	1.7(1)
Nd16	0.6190(6)	0.383(1)	0.3174(2)	−1.8(1)	0.4(1)	−1.7(1)

[a] Each atom is reproduced at $(x, y, z) + (1/2, 1/2, 0)$.

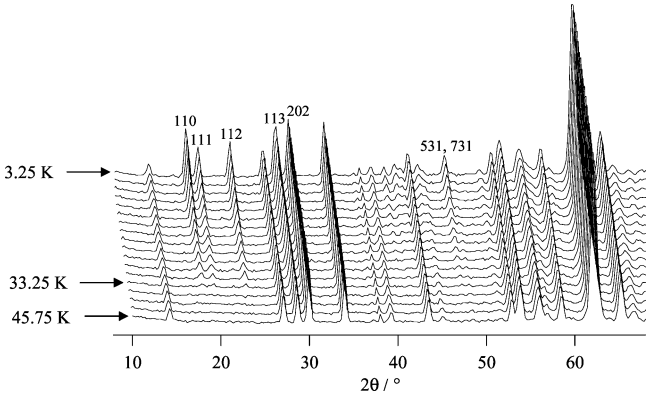

Figure 18. Neutron diffraction patterns of $Nd_2BaLiRuO_7$ as a function of temperature. Only principal magnetic peaks are labeled.

systems,[5,28−30] there is a considerable variation in the individual bond lengths. Warda et al. have previously observed a tetragonal distortion in the ordered $n = 1$ phases $La_2Li_{0.5}Ni_{0.5}O_4$,[15] and in a single-crystal study of $La_2Li_{0.5}Au_{0.5}O_4$, the LiO_6 octahedra were found to be so distorted the compound adopted a T′ phase in preference to the more common K_2NiF_4-type structure.[31] The environment around the Li cation in $Nd_2BaLiRuO_7$ is such that the two longest Li−O bonds within the octahedra lie almost perpendicular to the perovskite-like blocks, as was the case in $La_2Sr_2LiRuO_8$, with the bond to the oxide ion on the edge of the block being the longer of the pair.

There is a conflict between the structures refined from neutron and X-ray diffraction data and the electron diffraction data. To index the electron diffraction patterns, it is necessary to double the volume of the unit cell identified by X-ray and neutron diffraction. This strongly implies that the structure obtained from X-ray and neutron diffraction is averaged over the characteristic length scale of a neutron and X-ray diffraction experiment, whereas when examined over a shorter coherence length, the structure shows added complexity. The bond lengths discussed above must therefore be taken as mean bond lengths and the significance of the tabulated bond lengths is therefore limited. In other words, although long-range cation order persists over the neutron length scale, there is some unidentified feature that is only apparent when the structure is probed on a shorter length scale. The fact that the MAS NMR spectrum can be interpreted in terms of a single Li site suggests that the unidentified feature does not involve the alkali-metal cation.

In comparison with electron diffraction patterns and lattice images taken on other $n = 2$ phases, there is remarkably little evidence for imperfection in the microstructure of $Nd_2BaLiRuO_7$. We shall show in a subsequent paper that streaking in electron diffraction patterns points to the presence of defects in the ordered structures of $La_2BaLiRuO_7$ and $Pr_2BaLiRuO_7$. High-resolution lattice images have previously identified the disorder in the arrangement of the perovskite blocks along [001] in La_3LiMnO_7[7] and related $n = 1$ RP phases.[3,6]

The ^{7}Li MAS NMR spectra of $Nd_2BaLiRuO_7$ consisted of a single resonance accompanied by spinning sidebands and weak resonances from the lithium-containing impurities. The data were consistent with the presence of a single local environment for the lithium cations. In contrast to the case of $La_2Sr_2LiRuO_8$, there was no evidence for Li/Ru site inversion in the NMR spectrum. This is consistent with the high degree of structural coherence observed in the lattice images and the lower level of inversion (3.6%) derived from the diffraction data in this case compared to that of the $n = 1$ composition (7.4%). Together, these observations reinforce the hypothesis[6] that the inversion parameter derived from the diffraction data is a measure of the density of stacking faults rather than a measure of the concentration of local antisite defects. Previous studies on La_2LiRuO_6,[5] $La_2Sr_2LiRuO_8$,[6] and related B-site Li^+:Mn^{4+} RP phases[3,7] have shown that the size and sign of the hyperfine shifts can be rationalized by considering the arrangements of the paramagnetic ions in the local lithium environment. Two important mechanisms have been identified in La_2LiRuO_6 and related isoelectronic Mn(IV) compounds; the 90° interaction and the 180° interaction, resulting in hyperfine shifts between 250 and 300 ppm and −75 and −125 ppm respectively.[5,7,32] The 180° interaction involves the e_g orbital on the Ru^{5+} ions, and the 90° interaction involves the half-filled t_{2g} orbitals. Assuming 1:1 Li:Ru chessboard-type order within the perovskite blocks of $Nd_2BaLiRuO_7$, each Li^+ is connected to five Ru^{5+} ions. For a structure that contains 180° Li−O−Ru bond angles, a shift of approximately −625 ppm is predicted. The less negative observed hyperfine shift implies the presence of smaller Li−O−Ru bond angles,

(28) Stitzer, K. E.; Smith, M. D.; zur Loye, H.-C. *Solid State Sci.* **2002**, *4*, 311.
(29) Tortelier, J.; Gougeon, P. *Acta Crystallogr. Sect. C: Cryst. Struct. Commun.* **1996**, *52*, 500.
(30) Lopez, M. L.; Veiga, M. L.; Jerez, A.; Pico, C. *Mater. Res. Bull.* **1990**, *25*, 1271.
(31) Pietzuch, W.; Warda, S. A.; Massa, W.; Reinen, D. *Z. Anorg. Allg. Chem.* **2000**, *626*, 113.
(32) Pan, C.; Joo Lee, Y.; Ammundsen, B.; Grey, C. P. *Chem. Mater.* **2002**, *14*, 2289.

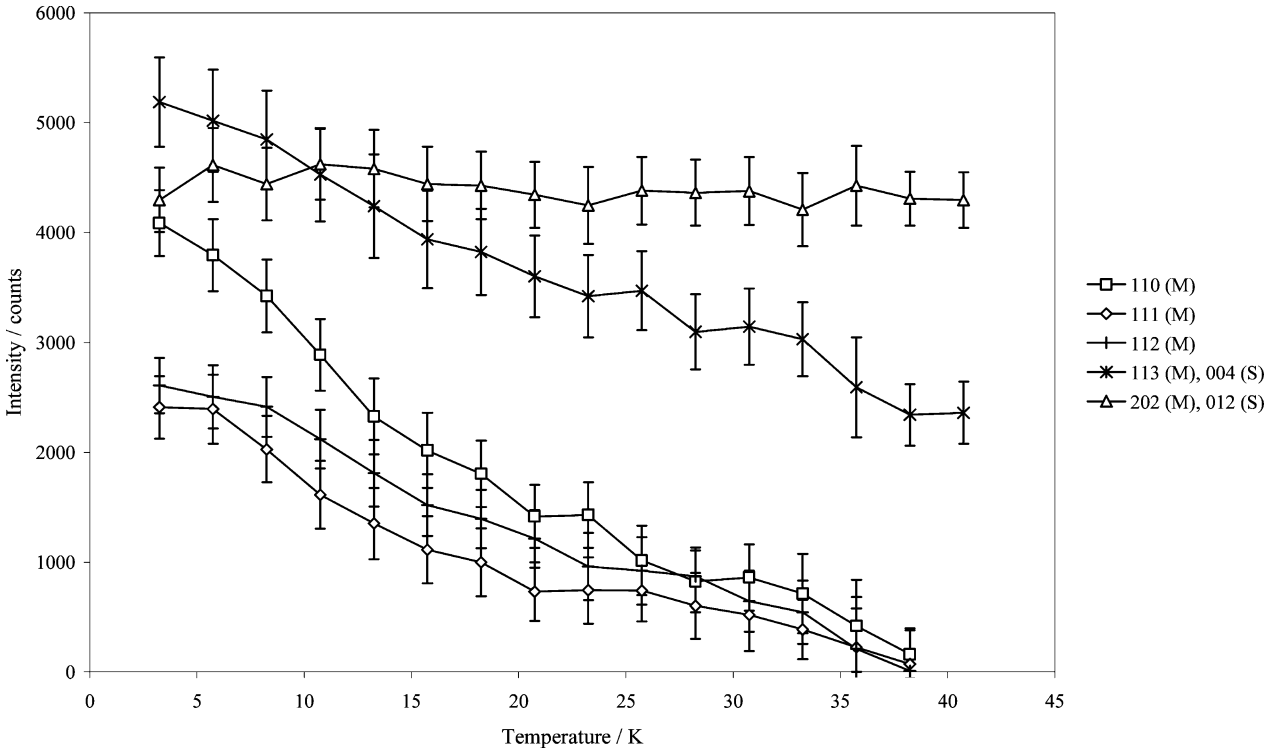

Figure 19. Temperature dependence of the intensity of magnetic reflections compared to structural reflections of $Nd_2BaLiRuO_7$.

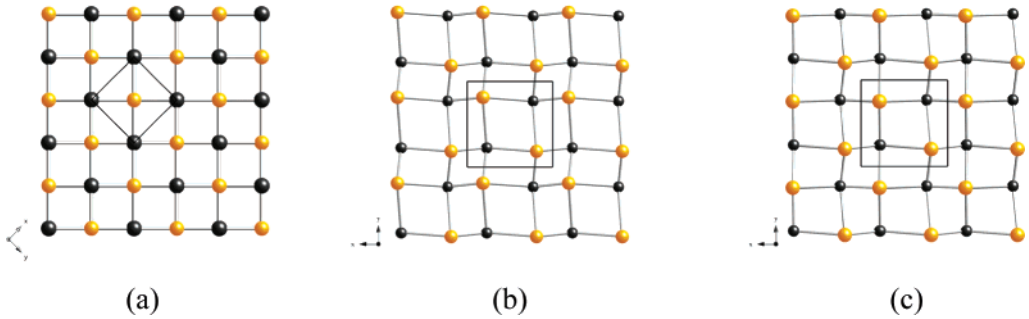

Figure 20. LnO layer for a (a) typical *I*4/*mmm*, $n = 2$ RP phase, (b) $La_2BaIn_2O_7$, and (c) $Nd_2BaLiRuO_7$.

which is consistent with the diffraction data. The small observed shift of $Nd_2BaLiRuO_7$ ($\delta = -14$ ppm) thus provides further evidence for the presence of tilted octahedra within the structure. However, it is plausible that an additional interaction with the unpaired electrons on the Nd^{3+} cations will also affect the Li shift, particularly since magnetic coupling between Ru and the rare-earth cation is observed at low temperatures. Such an interaction results in the observation[33,34] of large negative hyperfine shifts in the ^{119}Sn and ^{13}C NMR spectra of neodymium stannates and acetates, respectively.

The negative value of the Weiss constant (θ) indicates that the predominant magnetic interactions in $Nd_2BaLiRuO_7$ are antiferromagnetic. The Curie constant in the temperature range $65 \leq T/K \leq 300$ is only slightly lower than the value (5.15 $cm^3\ mol^{-1}\ K^{-1}$) calculated for a collection of paramagnetic Ru(V) and Nd^{3+} cations assuming that the Ru(V) cations show spin-only behavior and that the Nd^{3+} cations can be modeled using a single, Russell−Saunders *J* value. This result suggests that the outer electrons of the Ru(V) cations behave in a localized manner and thus contrasts with that reported for many other oxides, including $n = 1$ $La_2Sr_2LiRuO_8$, where an enhanced value of the effective magnetic moment of Ru(V), indicative of a shift toward itinerant electron behavior, was observed.[23] The variations in the behavior of the $4d^3$ species can be attributed, at least in part, to the differences in the acid−base properties of the various alkaline-earth and lanthanide cations that are present.

A change in the gradient of the magnetic susceptibility is observed at 40 K. We propose that this is a result of short-range antiferromagnetic ordering of the ruthenium moments within the individual perovskite blocks with, as yet, no significant interaction between neighboring blocks. The magnetic ordering present at this temperature thus occurs over too short a range to influence the neutron diffraction data. There is a further gradient change at 32 K which we take as evidence of the onset of 3-D antiferromagnetic ordering of the Ru cations both within and between the perovskite layers throughout the crystal. This interpretation is supported by the appearance of additional Bragg scattering

(33) Brough, A. R.; Grey, C. P.; Dobson, C. M. *J. Am. Chem. Soc.* **1993**, *115*, 7318.
(34) Grey, C. P.; Dobson, C. M.; Cheetham, A. K.; Jakeman, R. J. B. *J. Am. Chem. Soc.* **1989**, *111*, 505.

in the neutron diffraction pattern at 33 K (Figure 18). Confirmation that the initial ordering involves only the Ru cations was provided by the successful analysis of the neutron diffraction data collected at 20 K when only they were considered to contribute to the observed scattering. It can be seen from Figure 15 that not all the antiferromagnetic Ru−Ru interactions are satisfied in the magnetic structure. This frustration is likely to be one cause of the lowering of the Néel temperature on moving from $n = 1$ $La_2Sr_2LiRuO_8$ to $n = 2$ $Nd_2BaLiRuO_7$. Although the dimensionality of the crystal structure increases on making this change, the degree of frustration among NN interactions increases and the Néel temperature consequently decreases. A Néel temperature of ~30 K is typical for Ru^{5+}-containing phases which experience frustration on the ruthenium sublattice,[5,22,23,35] for example, the perovskite La_2LiRuO_6 orders antiferromagnetically at 30 K.[5] By comparison, the nonfrustrated Ru(V) compounds Ca_3LiRuO_6 and Sr_3LiRuO_6 have higher Néel temperatures of 120 and 90 K, respectively.[36] Battle et al. have suggested that the frustration within the perovskite phase La_2LiRuO_6 is the most significant factor in lowering the ordering temperature below those observed for the other phases. It was postulated that an ordering temperature of 100 K, as in Sr_3LiRuO_6, is a better indication of the inherent strength of the superexchange interactions between Ru cations[5] in an insulating oxide.

The maximum at 8 K in the susceptibility data is assigned to the long-range ordering of the rare-earth sublattice and this is confirmed by the successful refinement of a magnetic model containing both Ru and Nd against neutron data collected at low temperature. This is the first time a long-range magnetic structure has been observed and refined for an $n = 2$ RP phase in which there are magnetic cations present and ordered on both the A and B sites. While the antiferromagnetic ordering within the blocks is as predicted, the factors which determine the nature of the observed interblock coupling are less clear. Possibly the unknown structural distortion observed in the microscopy has an impact on the long-range order of the rare-earth moments. The ordered moment on the ruthenium at low temperatures (2.2(2) μ_B) is relatively large in comparison to other Ru^{5+} compounds;[22−24] however, the corresponding perovskite, La_2LiRuO_6, was also found to have an ordered moment of 2.2(2) μ_B.[5] The reduction from the spin-only value for Ru^{5+} (3 μ_B) can be attributed to the effect of covalency within the structure. The ordered moment on the Nd atoms at low temperatures was 2.53(8) μ_B. This value is similar to those observed in related materials,[27,37,38] but lower than the calculated value of 3.29 μ_B.

In conclusion, the A-site and B-site ordered $n = 2$ RP phase $Nd_2BaLiRuO_7$ has been synthesized and characterized, both structurally and magnetically. This compound is believed to be the first example of a fully cation-ordered $n = 2$ RP phase, and the first to show magnetic ordering on both the lanthanide and transition-metal sites. We shall report the structural and magnetic properties of the related phases $Pr_2BaLiRuO_7$, $La_2BaLiRuO_7$, and $NdPrBaLiRuO_7$ in future publications.

Acknowledgment. We thank EPSRC (a studentship for J.A.R.) and the Royal Society (a Research Fellowship for J.S.) for support. C.P.G. wishes to thank Younkee Paik and Nicolas Dupre with help with the NMR experiments and DMR0211353 for finanical support. We are grateful to Thomas Hansen for experimental assistance at ILL.

CM050923Z

(35) Battle, P. D.; Macklin, W. J. *J. Solid State Chem.* **1984**, *52*, 138.
(36) Darriet, J.; Grasset, F.; Battle, P. D. *Mater. Res. Bull.* **1997**, *32*, 139.
(37) Battle, P. D.; Green, M. A.; Laskey, N. S.; Millburn, J. E.; Radaelli, P. G.; Rosseinsky, M. J.; Sullivan, S. P.; Vente, J. F. *Phys. Rev. B* **1996**, *54*, 15967.
(38) Izumiyama, Y.; Doi, Y.; Wakeshima, M.; Hinatsu, Y.; Shimojo, Y.; Morii, Y. *J. Phys.: Condens. Matter* **2001**, *13*, 1303.